PCCP

PAPER

View Article Online
View Journal | View Issue

Cite this: *Phys. Chem. Chem. Phys.*, 2022, **24**, 16353

Antioxidant and copper-chelating power of new molecules suggested as multiple target agents against Alzheimer's disease. A theoretical comparative study†

Maciej Spiegel, [a] Tiziana Marino, [a] Mario Prejanò [b] and Nino Russo *[a]

Received 26th April 2022,
Accepted 12th June 2022

DOI: 10.1039/d2cp01918c

rsc.li/pccp

In this study, the scavenging activity against OOH radicals and the copper-chelating ability of two new synthesized molecules (named **L1** and **L2**) that can act as multiple target agents against Alzheimer's disease have been investigated at the density functional theory level. The pK_a and molar fractions at physiological pH have been predicted. The main antioxidant reaction mechanisms in lipid-like and water environments have been considered and the relative rate constants determined. The copper-chelating ability of the two compounds has also been explored at different coordination sites and computing the complexation kinetic constants. Results show the $\mathbf{L_1}$ compound is a more effective radical scavenging and copper-chelating agent than $\mathbf{L_2}$.

Introduction

Alzheimer's disease (AD), first described in 1906, is a serious neurodegenerative disorder that induces progressive memory loss, devastating the quality of life of patients, and is the leading cause of death worldwide. It is an age-dependent disease that occurs generally after the age of 65 years. With the increase in life expectancy in the most industrialized countries, it has become one of the most widespread diseases in the world. In 2015, AD affected nearly 50 million people, and the latest estimates predict that it will grow to around 135 million in 2050.[1] The estimated economic cost of this disease is enormous and is set to increase dramatically. Suffice it to say that in the UK alone, the cost of caring for people with AD will reach £66 billion in 2050.[2]

The pathology of AD is essentially characterized by the accumulation of senile plaques and neurofibrillary tangles and by abnormal levels of neurotransmitters.[3–5] The senile plaques are formed by insoluble peptide segments composed of 39–43 amino acids (Aβ), and their aggregation (amyloid cascade hypothesis) and the possibility of the formation of small and soluble oligomers (oligomer hypothesis) are considered important phenomena and the basis of the disease.[6,7] Despite the great amount of research carried out over the past twenty years, the exact cause of AD is still poorly understood and an effective cure has not yet been proposed.[3,4,8,9] The few drugs approved by the US FDA and other European and Asian agencies essentially serve to alleviate the symptoms of the disease and improve the quality of life of patients, but they are ineffective in slowing down its evolution.[10] For these reasons, the development of research in the field of AD is fundamental to both a better understanding of the mechanisms underlying its onset and the proposal of new, more effective and targeted drugs.

Autopsy examination of the brain tissues of patients who died due to AD has shown the presence of high and abnormal concentrations of metals such as copper, zinc and iron ions (about six and three times the normal quantity in the human brain, for Cu, and for Zn and Fe, respectively).[11–13] It has been shown that this metal ion dyshomeostatis can play an important role since the formation of toxic metal–amyloid complexes promotes Aβ aggregation.[13] Furthermore, owing to the redox nature of the metal ions involved, the presence of molecular oxygen in the brain tissue leads to the formation of reactive oxygen species (ROS) through Fenton-like reactions with a consequent increase in oxidative stress. In fact, due to the occurrence of high levels of unsaturated fatty acids (the preferred target of attack for ROS), the brain is particularly sensitive to oxidative stress, as has been proved in different neurodegenerative diseases.[13–15]

Among the three metal ions that undergo dyshomeostatis in the brains of AD patients, the most involved ions seem to be Cu^{2+} and Zn^{2+}, which form stable complexes with the Aβ[16] proteins, with different and much higher stability constants in the case of Cu^{2+}.[17,18]

[a] *Dipartimento di Chimica e Tecnologie Chimiche, Università della Calabria, I-87136 Rende, CS, Italy. E-mail: nrusso@unical.it*
[b] *Department of Organic Chemistry, Arrhenius Laboratory, Stockholm University, Stockholm, SE-10691, Sweden*

† Electronic supplementary information (ESI) available. See DOI: https://doi.org/10.1039/d2cp01918c

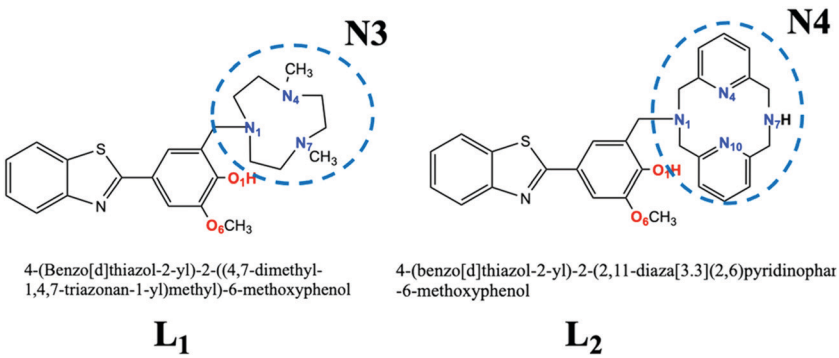

Scheme 1 Chemical structure of the bifunctional chelators investigated. The atoms coloured represent the metal chelating sites considered in the present work.

A strategy to limit ROS damage is based on the use of chelator agents that are able to control the increase in the concentration of metals, and to increase the level of antioxidant substances that are not usually present in the brain in sufficient quantities so as to counteract the effects caused by the rise in concentration of free radicals.[19,20]

On the basis of the observations reported above, the proposal of new drugs endowed with multiple actions in the latest research can contribute to increasing our knowledge not only about degenerative diseases, including Alzheimer's, but also to their treatment using multiple actions.[21–23]

Very recently, Cho *et al.*[24] proposed some multifunctional molecular systems whose structure provided an antioxidant action together with a chelating action, to reduce the concentration of the copper ions in the brain ($\mathbf{L_1}$ and $\mathbf{L_2}$ of Scheme 1). The first action is due to the presence of a guaiacyl group, while some nitrogenous chelating groups, of different sizes that can coordinate the Cu^{2+} ion, express the second. Furthermore, some of their derivatives form stable Cu-radiolabeled complexes.[25] These systems, which show values of lipophilicity such that their brain barrier penetration is possible, have been chemically characterized, and *in vivo* tests have suggested them as promising drugs against AD.

A better knowledge of their structural and electronic properties, as well as of their biological mechanisms, is very useful for their proposition as lead compounds for the development of new therapies in the treatment of AD. For these reasons, we have undertaken a detailed theoretical study using the density functional theory (DFT), which has proved to be particularly useful in the study and prediction of various molecular properties and reaction mechanisms, even in systems containing transition metals.[26] In particular, we have considered different antioxidant reaction paths to establish what kind of scavenging mechanism these molecules follow and the possible chelating sites for copper-ion coordination.

Computational details

Geometry optimizations and frequency calculations were performed using the Gaussian 09[27] package in the framework of DFT. The M05 exchange–correlation functional[28] in conjunction with the 6-31+G(d,p) basis set and the SMD solvation model,[29] to mimic lipid-like (ε = 4.7, pentyl ethanoate (PE)) and water environments (ε = 78.48), has been used. In order to improve the electronic energies, single-point computations on previously optimized geometries have been recalculated using the 6-311+G(d,p) basis sets. The unrestricted formalism has been employed for the treatment of radical species. The intrinsic reaction coordinate (IRC) procedure has been applied to verify that the intercepted transition state is properly connected to the relative minima (reactant and product) in the minimum-energy reaction path. The quantum mechanism-based method QM-ORSA,[30,31] which is based on conventional transition state theory[32,33] and Marcus theory,[34] has been used. The computed rate constants, within or close to the diffusion-limited regime, have been corrected using Collins–Kimball theory.[35]

The computational procedure previously described[36] has been applied to obtain the molar fraction and pK_a values. Numerous previous studies have demonstrated, in fact, that this computational protocol gives reliable results for thermochemistry and kinetics parameters relative to reactions involving free radicals and metals.[37–40]

Results and discussion

Primary antioxidant properties

From experimental studies on the protonation constants of 1,4,7-triazacyclononane and its derivatives, a high pK_1 value related to protonation of the amino group (10.44) indicates that the neutral form is the preferred one.[41] This evidence prompted us to consider the amino group of the macrocycle (N3; Scheme 1) in the neutral form and, by analogy, the macrocycle (N4; Scheme 1) is also considered to be deprotonated. Due to the lack of any experimental information on the pK_a of the 2-phenylbenzothiazole fragment considered in both systems, as a first step of this work we calculated the pK_a and the molar fractions at physiological pH (7.4). The results depicted in Fig. 1 show that the pK_a values of the two systems are similar, although that of $\mathbf{L_1}$ is slightly lower than $\mathbf{L_2}$ (8.57 *versus* 9.22). For both the equilibria, at physiological pH the dominant form is the neutral one with the monoanion species assuming percentages of 6.3 and 1.5 for $\mathbf{L_1}$ and $\mathbf{L_2}$, respectively. Although these are smaller values for the dissociated form, they have

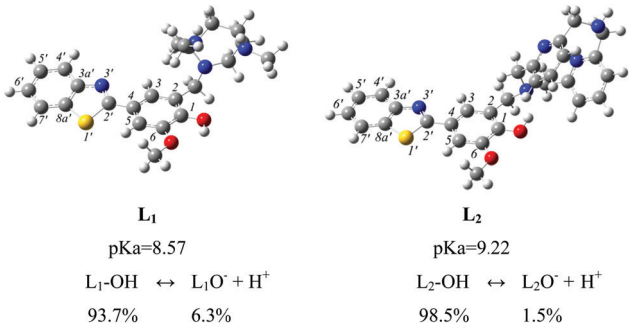

Fig. 1 Optimized structures, dissociation constants and molar distribution at pH = 7.4 for $\mathbf{L_1}$ and $\mathbf{L_2}$ molecules.

been taken into account in the computation of the antioxidant properties.

Based on our previous experience[42,43] and that of other research groups,[39,40,44–46] the following redox and non-redox pathways were explored:

$$\text{Hydrogen atom transfer (HAT): } HX + R^{\bullet} \rightarrow X^{\bullet} + RH$$

$$\text{Single electron transfer (SET): } HX + R^{\bullet} \rightarrow HX^{+\bullet} + R^{-}$$

$$\text{Radical adduct formation (RAF): } HX + R^{\bullet} \rightarrow [HX{-}R]^{\bullet}$$

The obtained Gibbs free energies of reaction are collected in Table 1. In both the considered environments and for both the considered species, the RAF mechanism generates endergonic reactions with Gibbs free energies higher than 10 kcal mol^{-1}, suggesting that they do not take place. In addition, the SET mechanism in a lipid-like environment appears to be highly unlikely given the high endothermic values of the reaction Gibbs free energies. In the aqueous phase, calculations for both neutral and deprotonated forms confirm the feasibility of the SET mechanism. In fact, for the former we find ΔG values of 9.6 and 7.5 kcal mol^{-1} for $\mathbf{L_1}$ and $\mathbf{L_2}$, respectively, while for the latter they become −0.6 kcal mol^{-1} for $\mathbf{L_1}$ and 0.1 kcal mol^{-1} for $\mathbf{L_2}$.

Table 1 Gibbs free energies (kcal mol^{-1}) of the studied reaction channels for $\mathbf{L_1}$ and $\mathbf{L_2}$ against the OOH radical in pentyl ethanoate (PE) and water (W) environments

Mechanism	$\mathbf{L_{1(PE)}}$ ($\mathbf{L_{2(PE)}}$)	$\mathbf{L_{1(W)}}$ ($\mathbf{L_{2(W)}}$)	$\mathbf{L_1}^-_{(W)}$ ($\mathbf{L_2}^-_{(W)}$)
HAT	−4.1 (−3.5)	−9.6 (−6.9)	—
RAF-C1	18.2 (19.0)	14.2 (16.9)	18.3 (17.5)
RAF-C2	24.8 (31.0)	24.7 (30.3)	21.5 (21.5)
RAF-C3	18.0 (14.9)	16.7 (17.5)	18.9 (18.5)
RAF-C4	25.5 (24.8)	24.0 (24.0)	21.9 (21.2)
RAF-C5	22.2 (22.5)	20.3 (21.6)	19.4 (19.5)
RAF-C6	20.0 (22.8)	18.8 (22.0)	11.7 (16.4)
RAF-C2′	20.6 (18.2)	15.9 (17.3)	17.9 (19.9)
RAF-C3a′	32.9 (33.8)	29.2 (30.5)	27.6 (29.5)
RAF-C4′	17.9 (17.8)	15.3 (16.4)	15.2 (13.9)
RAF-C5′	22.3 (22.2)	20.6 (21.2)	20.4 (19.7)
RAF-C6′	18.3 (18.7)	17.5 (18.4)	16.8 (16.4)
RAF-C7′	18.3 (18.6)	16.9 (17.9)	17.5 (17.0)
RAF-C7a′	27.9 (27.7)	25.9 (27.1)	24.4 (25.1)
SET	45.8 (67.3)	9.6 (7.5)	−0.6 (0.1)

Analyzing the data for the HAT mechanism, we note that, in both environments, the ΔG values indicate exergonic reactions for both the studied compounds. In particular, those related to the aqueous medium assume exothermic values (−9.6 and −6.9 kcal mol^{-1} for $\mathbf{L_1}$ and $\mathbf{L_2}$, respectively).

Based on the ΔG values obtained for the various reaction mechanisms, we proceeded to determine the potential energy surfaces by characterizing the transition states and the products for those processes whose reaction energies result in being lower than 10 kcal mol^{-1}. The results, reported in Table 2 and Fig. 2, indicate that in the lipid-like phase, for both systems, only the HAT mechanism is possible with energy barriers of 15.0 and 19.1 kcal mol^{-1}, for $\mathbf{L_1}$ and $\mathbf{L_2}$, respectively. In the aqueous environment, for the neutral forms of both compounds, the reactions that occur with SET and HAT mechanisms are energetically feasible. In particular, the energy barriers for $\mathbf{L_1}$ turn out to be 11.9 (SET) and 15.4 kcal mol^{-1} (HAT). Those found for $\mathbf{L_2}$ are 11.2 and 22.4 kcal mol^{-1} for the SET and HAT channels, respectively. Finally, the only possible path for both the anionic compounds results in being the SET mechanism, for which a barrier of 3.3 kcal mol^{-1} for $\mathbf{L_1}$ (3.6 kcal mol^{-1} for $\mathbf{L_2}$) must be overcome. The transition-state structures for the HAT mechanism, reported in Fig. 2, show similar geometrical parameters for the H transfer from the OH–$\mathbf{L_1}$ ($\mathbf{L_2}$) to the OOH radical in both the considered environments. The analysis of the computed negative frequency accounts for this process satisfactorily.

The obtained kinetic rate constants (Table 3) in the PE solvent for the HAT path indicate that the $\mathbf{L_1}$ system is a better antioxidant than the $\mathbf{L_2}$ system, with their k values being 1.89×10^4 and 7.43×10^1 M^{-1} s^{-1}, respectively. Comparison with the corresponding k value (3.40×10^3 M^{-1} s^{-1}) of Trolox (generally used as reference antioxidant)[31,47] suggests that $\mathbf{L_1}$ is a more efficient OOH scavenger than $\mathbf{L_2}$.

In water and at physiological pH (7.4) the situation is different. In particular, we underline that, in the neutral form, which has a higher molar fraction (93.7 and 98.5% for $\mathbf{L_1}$ and $\mathbf{L_2}$, respectively), the HAT mechanism in $\mathbf{L_1}$ (k = 1.02×10^5 M^{-1} s^{-1}) is preferred, while the SET mechanism dominates

Table 2 Gibbs (ΔG) and activation energies ($\Delta G^{\ddagger}$) for the feasible reaction channels for $\mathbf{L_1}$ ($\mathbf{L_2}$) reacting with an OOH radical in pentyl ethanoate (PE) and water (W) environments. All data are in kcal mol^{-1}

	$\mathbf{L_{1(PE)}}$ ($\mathbf{L_{2(PE)}}$)		$\mathbf{L_{1(W)}}$ ($\mathbf{L_{2(W)}}$)		$\mathbf{L_1}^-_{(W)}$ ($\mathbf{L_2}^-_{(W)}$)	
Mechanism	ΔG	$\Delta G^{\ddagger}$	ΔG	$\Delta G^{\ddagger}$	ΔG	$\Delta G^{\ddagger}$
HAT	−4.1 (−3.5)	15.0 (19.1)	−9.6 (−6.9)	15.4 (22.4)	—	
SET	45.8 (67.3)	52.3 (194.0)	9.6 (7.5)	11.9 (11.2)	−0.6 (0.1)	3.3 (3.6)

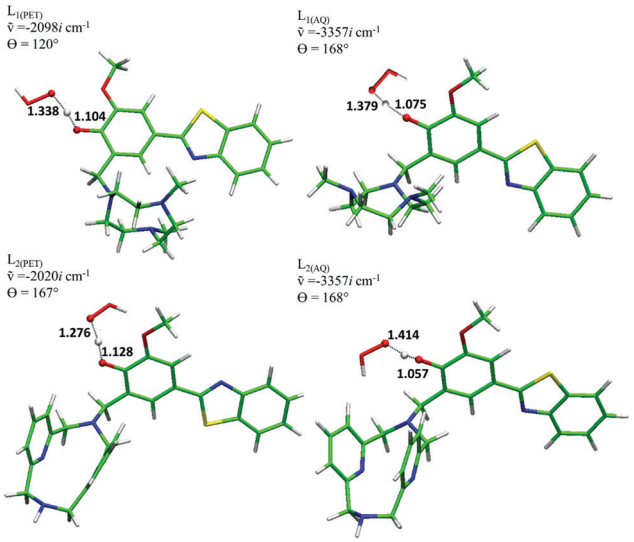

Fig. 2 $\mathbf{L_1}$ and $\mathbf{L_2}$ transition-state structures for the HAT mechanism with the corresponding frequencies, main bond lengths (Å), and dihedral angles (degrees).

Table 3 Rate constants (k) and branching ratios (Γ) for the reaction between $\mathbf{L_1}$ and $\mathbf{L_2}$ ligands and the OOH radical (at 298.15 K) in pentyl ethanoate (PE) and water (W) environments

	k (M^{-1} s^{-1})	Γ (%)	k (M^{-1} s^{-1})	Γ (%)	k (M^{-1} s^{-1})	Γ (%)
Mechanism	$\mathbf{L_{1(PE)}}$		$\mathbf{L_{1(W)}}$		$\mathbf{L_1}^-$(W)	
HAT	1.89×10^4	100.00	1.02×10^5	89.87		
SET			1.15×10^4	10.13	2.51×10^{10}	100.00
F	100%		93.7%		6.3%	
k_{total}	1.89×10^4		1.14×10^5		2.51×10^{10}	
fk_{total}			1.07×10^5		1.58×10^9	
	$\mathbf{L_{2(PE)}}$		$\mathbf{L_{2(W)}}$		$\mathbf{L_2}^-$(W)	
HAT	7.43×10^1	100.00	1.22×10^2	3.39		
SET			3.59×10^4	96.61	1.49×10^{10}	100.00
F	100%		98.5%		1.5%	
k_{total}	7.43×10^1		3.60×10^4		1.49×10^{10}	
fk_{total}			3.55×10^4		2.24×10^8	

for the $\mathbf{L_2}$ species ($k = 3.59 \times 10^4$ M^{-1} s^{-1}). Looking at the k_{total} values, our data indicate that $\mathbf{L_1}$ is a better radical scavenger than $\mathbf{L_2}$ with a difference of one order of magnitude. The comparison with Trolox in the aqueous solvent and under physiological pH conditions ($k = 8.96 \times 10^4$ M^{-1} s^{-1})[46] shows that $\mathbf{L_1}$ is more efficient, while $\mathbf{L_2}$ has almost the same antioxidant power.

Our results well agree with the experimental measurements that reveal $\mathbf{L_1}$ to be 1.6 times more efficient than Trolox as a radical-scavenging system.[25]

Secondary antioxidant properties

In this section, we report the results concerning the Cu^{2+} complexation abilities of $\mathbf{L_1}$ and $\mathbf{L_2}$ throughout the computation of Gibbs free energies (ΔG_f) for the following reactions:

$$Cu(H_2O)_6{}^{2+} + L \rightarrow [Cu(H_2O)_6\ L]^{2+}$$

$$Cu(H_2O)_6{}^{2+} + L^- \rightarrow [Cu(H_2O)_6\ L]^{+}$$

Table 4 Gibbs formation energies (ΔG_f), their differences ($\Delta\Delta G_f$) and kinetic constants (K_f, ΣK_f, K_f^{II} and K_f^{app}) for the different coordination's sites of $\mathbf{L_1}$ and $\mathbf{L_2}$

Coordination site	ΔG_f (kcal mol^{-1})	$\Delta\Delta G_f$ (kcal mol^{-1})	K_f	ΣK_f (K_f^{II})
$\mathbf{L_1}$ (93.7%)				
N3	−18.4	1.2	2.88×10^{13}	
N,O	−19.6	0.0	2.24×10^{14}	
O,O	−5.8	13.8	1.61×10^4	
				2.53×10^{14} (2.37×10^{14})
$\mathbf{L_1}^-$ (6.3%)				
N3	−25.2	11.2	2.81×10^{18}	
N,O	−36.4	0.0	5.01×10^{26}	
O,O	−16.2	20.2	7.11×10^{11}	
				5.01×10^{26} (3.16×10^{25})
K_f^{app} ($\mathbf{L_1}$) = 3.16×10^{25}				
$\mathbf{L_2}$ (98.5%)				
N4	−13.7	0.0	1.21×10^{10}	
O,O	4.4	18.1	6.38×10^4	
				1.21×10^{10} (1.19×10^{10})
$\mathbf{L_2}^-$ (1.5%)				
N4	−11.5	1.6	2.68×10^8	
O,O	−13.1	0.0	4.58×10^9	
				6.44×10^{18} (9.66×10^{16})
K_f^{app} ($\mathbf{L_2}$) = 9.66×10^{16}				

For both the ligands we have considered three possible coordination sites of the Cu^{2+} ion (Scheme 1): coordination with the O_1 and O_6 oxygen atoms linked in the phenolic cycle, with the nitrogen atoms of the peripheral macrocycle (N3 or N4 for $\mathbf{L_1}$ and $\mathbf{L_2}$, respectively) and with both sites (the oxygen atoms of the phenyl ring and the nitrogen atoms of the macrocycle (N3 or N4 for $\mathbf{L_1}$ and $\mathbf{L_2}$)). This topology will hereafter be referred to as O,O, N3 (or N4), and N,O. The energetic values (ΔG and $\Delta\Delta G$) and the main geometrical parameters around the copper ion are reported in Table 4 and Table S1 (ESI†), respectively. The optimized structures are given in Fig. 3 (for $\mathbf{L_1}$) and Fig. 4 (for $\mathbf{L_2}$).

For $\mathbf{L_1}$, Table 4 shows that the preferred coordination site is N,O followed by N3 at only 1.2 kcal mol^{-1}. The O,O topology results in being at a higher energy (13.8 kcal mol^{-1}). For N,O coordination, analysis of the Cu–X bond lengths (Fig. 3 and 4 and Table S1, ESI†) reveals that the Cu ion interacts with the three nitrogen atoms of the peripheral macrocycle, while the bond with the O_1 oxygen is weak since Cu–O_1 assumes a value of 2.812 Å. In addition, the Cu^{2+} interacts with the two water molecules at distances of 2.084 and 2.355 Å. The situation is slightly different for the interaction with the anionic ligand. In fact, although the preferred coordination continues to be N,O, the other two are at higher energies (11.2 and 20.2 kcal mol^{-1} for N3 and O,O, respectively). In the absolute minimum, the Cu–O_1 bond is strong (Cu–O distance is 1.957 Å) due to the presence of a more negative charge on the interacting oxygen atom, and the solvation water molecules are away from the metal center (more than 3.1 Å).

Analysis of the spin density maps reveals that in the N,O coordination mode, for both the Cu–$\mathbf{L_1}$ and Cu–$\mathbf{L_1}^-$ systems

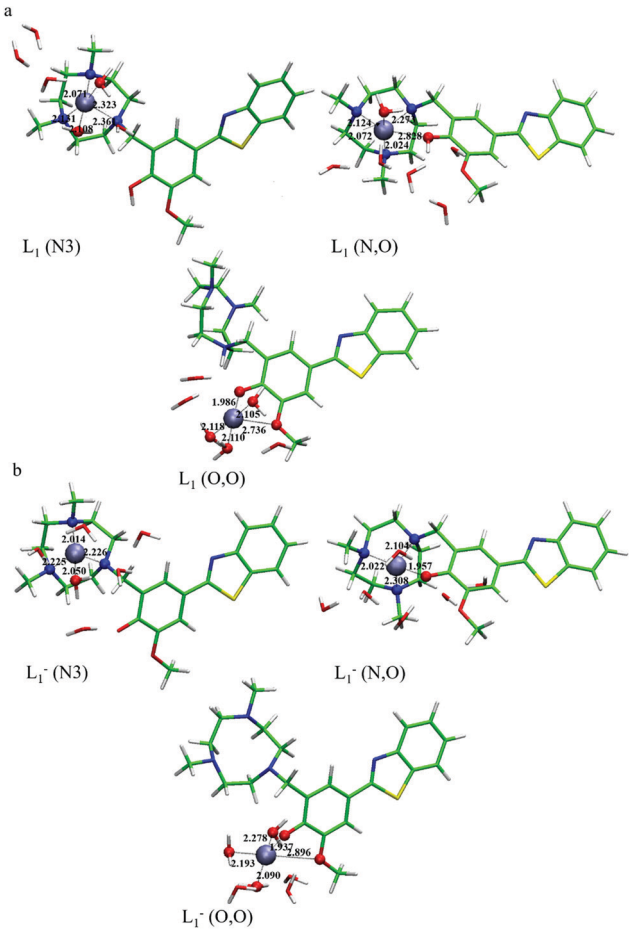

Fig. 3 Optimized structures for Cu–$\mathbf{L_1}$ (a) and Cu–$\mathbf{L_1}^-$ (b) complexes. Distances are in Å.

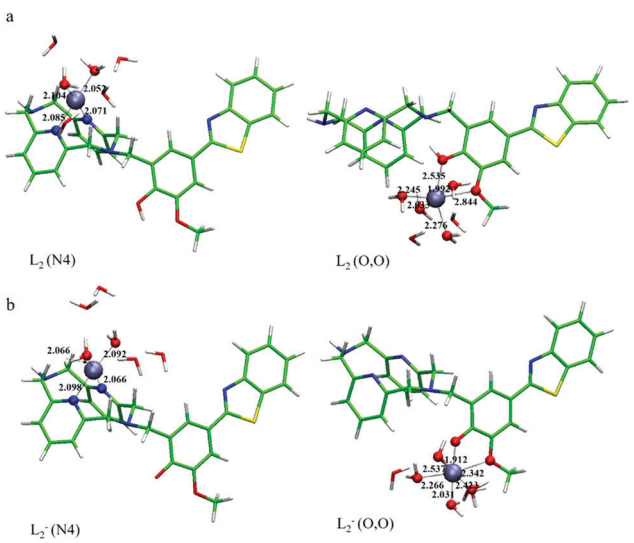

Fig. 4 Optimized structures for Cu–$\mathbf{L_2}$ (a) and Cu–$\mathbf{L_2}^-$ (b) complexes. Distances are in Å.

(see Fig. S1 and S2, ESI†), the spin density is almost distributed on the entire molecule, enhancing the stability of this conformation.

To discuss the complexation process for the $\mathbf{L_2}$ ligand, we note that for both the considered species, the N,O coordination is not a minimum in the potential energy surfaces. For the $\mathbf{L_2}$ neutral species the N4 topology is preferred over the O,O topology by 18.1 kcal mol^{-1} (see Table 4). From Table S1 (ESI†) and Fig. 4 it is possible to see that the Cu^{2+} ion is bonded with the N_4 and N_{10} nitrogen atoms of the pyridinophane ring (2.085 and 2.073 Å for Cu–N_4 and Cu–N_{10} bonds, respectively) and with the oxygen atoms of two water molecules with bond distances of about 2.0–2.1 Å. For the anionic form of $\mathbf{L_2}$, the preferred coordination site results in being the O,O topology while the N4 lies at only 1.6 kcal mol^{-1}. In the O,O mode, the copper ion forms two bonds with the O_1 and O_6 atoms of the phenyl ring, assuming the values of 1.918 Å (Cu–O_1) and 2.343 Å (Cu–O_6). There are two other strong interactions with the oxygen atoms of two water molecules with bond distances of 2.031 and 2.244 Å.

For both anionic species ($\mathbf{L_1}^-$ and $\mathbf{L_2}^-$) in the O,O topology the copper ion shows an octahedral coordination geometry.

Furthermore, the spin density behavior reveals in the neutral complex (Fig. S1, ESI†) that the resulting distribution with N4 coordination being shared in the two molecular fragments, whereas with O,O chelation it is more localized. In the charged complexes (Fig. S2, ESI†) spin delocalization is found, for both coordination modes, in only one segment, in agreement with the small energy difference between the complexes.

Comparing the molecular electrostatic potential of the $\mathbf{L_1}$ and $\mathbf{L_2}$ complexes (Fig. S3, ESI†) it is possible to note that in the $\mathbf{L_1}$ ligand the negative charge is mainly concentrated on the N3 site while in the $\mathbf{L_2}$ ligand, albeit to only a minor extent, the other fragment is also implicated. This distribution can be correlated with the fact that in $\mathbf{L_1}$ the preferred coordination site is the N,O.

According to the data gathered in Table 4, for the chelation processes predicted to be viable from a thermochemical point of view (exergonic or slightly endergonic reaction pathways) we computed the complexation kinetic constants according to a previously suggested procedure[48] and taking into account the populations of the complexes estimated through the Maxwell–Boltzmann distribution (see Table 4).

The obtained apparent equilibrium constants (K_f^{app}) for the $\mathbf{L_1}$ and $\mathbf{L_2}$ ligands were found to be 3.16×10^{25} and 9.66×10^{16} M^{-1}, respectively, indicating that the former is predicted to be a stronger Cu(II)-chelating agent that can reduce the Cu(II) free ions produced by the Fenton reactions associated with Alzheimer's disease.

Conclusions

A careful quantum mechanical study on the antioxidant and copper-chelating power of two new molecules, proposed as combined multiple target agents against Alzheimer's disease, has been performed in the framework of density functional theory. From our results, the following conclusions can be drawn:

The computed pK_a values of the methoxyphenol group present in the 2-phenylbenzothiazole moiety show a higher value for the $\mathbf{L_2}$ species. The molar distribution at physiological pH indicates that for both molecules the neutral form is dominant. However, the anionic species, although present at a small concentration, should be considered for their contribution to both the antioxidant and Cu-chelating properties.

In lipid-like and water environments, the HAT mechanism results in being exergonic.

The obtained rate constants clearly indicate that $\mathbf{L_1}$ is much more efficient than $\mathbf{L_2}$ as an OOH scavenger in both the studied environments and that $\mathbf{L_1}$ is more efficient than Trolox, which is generally used as a reference antioxidant.

The Cu^{2+} preferred coordination sites have been determined. The computed apparent equilibrium constants clearly show that the $\mathbf{L_1}$ ligand is much more efficient as a chelating agent.

Our results well agree with the available experimental indications.

We hope that our results can further stimulate other investigations devoted to the possible use of these systems as multiple target drugs against Alzheimer's disease.

Author contributions

All authors contributed equally to this work and have approved the final version of the manuscript.

Conflicts of interest

The authors declare no competing financial interest.

Acknowledgements

This research was supported in part by PLGrid Infrastructure (grant ID: plgantioxidants). The authors thank the Dipartimento di Chimica e Tecnologie Chimiche, Università della Calabria for the support.

References

1 T. P. C. Chierrito, S. P. Mantoani, C. Roca, C. Requena, V. Sebastian-Perez, W. O. Castillo, N. C. S. Moreira, C. Pérez, E. T. Sakamoto-Hojo, C. S. Takahashi, J. Jiménez-Barbero, F. J. Cañada, N. E. Campillo, A. Martinez and I. Carvalho, From dual binding site acetylcholinesterase inhibitors to allosteric modulators: A new avenue for disease-modifying drugs in Alzheimer's disease, *Eur. J. Med. Chem.*, 2017, **139**, 773–791.

2 F. Lewis, S. K. Schaffer and J. Sussex, *Alzheimer's Research*, UK, 2014, vol. 1, pp. 1–62.

3 S. J. C. Lee, E. Nam, H. J. Lee, M. G. Savelieff and M. H. Lim, Towards an understanding of amyloid-β oligomers: characterization, toxicity mechanisms, and inhibitors, *Chem. Soc. Rev.*, 2017, **46**, 310–323.

4 M. G. Savelieff, G. Nam, J. Kang, H. J. Lee, M. Lee and M. H. Lim, Development of Multifunctional Molecules as Potential Therapeutic Candidates for Alzheimer's Disease, Parkinson's Disease, and Amyotrophic Lateral Sclerosis in the Last Decade, *Chem. Rev.*, 2019, **119**, 1221–1322.

5 C. Lane, J. Hardy and J. Schott, Alzheimer's disease, *Eur. J. Neurol.*, 2018, **25**, 59–70.

6 S. Tiwari, V. Atluri, A. Kaushik, A. Yndart and M. Nair, Alzheimer's disease: pathogenesis, diagnostics, and therapeutics, *Int. J. Nanomed.*, 2019, **14**, 5541–5554.

7 Z. He, J. L. Guo, J. D. McBride, S. Narasimhan, H. Kim, L. Changolkar, B. Zhang, R. J. Gathagan, C. Yue, C. Dengler, A. Stieber, M. Nitla, D. A. Coulter, T. Abel, K. R. Brunden, J. Q. Trojanowski and V. M. Y. Lee, Amyloid-β plaques enhance Alzheimer's brain tau-seeded pathologies by facilitating neuritic plaque tau aggregation, *Nat. Med.*, 2018, **24**, 29–34.

8 L. Blaikie, G. Kay and P. K. T. Lin, Current and emerging therapeutic targets of alzheimer's disease for the design of multi-target directed ligands, *Med. Chem. Commun.*, 2019, **10**, 2052–2072.

9 J. Nasica-Labouze, P. H. Nguyen, F. Sterpone, O. Berthoumieu, N.-V. Buchete, S. Coté, A. De Simone, A. J. Doig, P. Faller, A. Garcia, A. Laio, M. S. Li, S. Melchionna, N. Mousseau, Y. Mu, A. Paravastu, S. Pasquali, D. J. Rosenman, B. Strodel, B. Tarus, J. H. Viles, T. Zhang, C. Wang and P. Derreumaux, Amyloid β Protein and Alzheimer's Disease: When Computer Simulations Complement Experimental Studies, *Chem. Rev.*, 2015, **115**, 3518–3563.

10 E. von Schaper, Everything but amyloid: new thinking prompts FDA revamp, *Nat. Biotechnol.*, 2018, **36**, 483–484.

11 Y. Liu, M. Nguyen, A. Robert and B. Meunier, Metal Ions in Alzheimer's Disease: A Key Role or Not?, *Acc. Chem. Res.*, 2019, **52**, 2026–2035.

12 K. P. Kepp, Bioinorganic chemistry of Alzheimer's disease, *Chem. Rev.*, 2012, **112**, 5193–5239.

13 M. A. Lovell, J. D. Robertson, W. J. Teesdale, J. L. Campbell and W. R. Markesbery, Copper, iron and zinc in Alzheimer's disease senile plaques, *J. Neurol. Sci.*, 1998, **158**, 47–52.

14 C. Cheignon, M. Tomas, D. Bonnefont-Rousselot, P. Faller, C. Hureau and F. Collin, Oxidative stress and the amyloid beta peptide in Alzheimer's disease, *Redox Biol.*, 2018, **14**, 450–464.

15 M. A. Greenough, J. Camakaris and A. I. Bush, Metal Dyshomeostasis and Oxidative Stress in Alzheimer's Disease, *Neurochem. Int.*, 2013, **62**, 540–555.

16 E. Atrian-Blasco, E. Cerrada, P. Faller, M. Laguna and C. Hureau, Role of PTA in the prevention of Cu(amyloid-b) induced ROS formation and amyloid-b oligomerisation in the presence of Zn, *Metallomics*, 2019, **11**, 1154–1161.

17 B. Alies, E. Renaglia, M. Rozga, W. Bal, P. Faller and C. Hureau, Cu(II) Affinity for the Alzheimer's Peptide: Tyrosine Fluorescence Studies Revisited, *Anal. Chem.*, 2013, **85**, 1501–1508.

18 T. R. Young, A. Kirchner, A. G. Wedd and Z. Xiao, An integrated study of the affinities of the Aβ16 peptide for Cu(I) and Cu(II): implications for the catalytic production of reactive oxygen species, *Metallomics*, 2014, **6**, 505–517.

19 J. T. Pedersen, K. Teilum, N. H. H. Heegaard, J. Østergaard, H.-W. Adolph and L. Hemmingsen, Rapid Formation of a Preoligomeric Peptide–Metal–Peptide Complex Following

Copper(II) Binding to Amyloid β Peptides, *Angew. Chem., Int. Ed.*, 2011, **50**, 2532–2535.
20 A. K. Sharma, S. T. Pavlova, J. Kim, J. Kim and L. M. Mirica, The effect of Cu2+ and Zn2+ on the Aβ42 peptide aggregation and cellular toxicity, *Metallomics*, 2013, **5**, 1529–1536.
21 M. W. Beck, J. S. Derrick, R. A. Kerr, S. B. Oh, W. J. Cho, S. J. C. Lee, Y. Ji, J. Han, Z. A. Tehrani, N. Suh, S. Kim, S. D. Larsen, K. S. Kim, J. Y. Lee, B. T. Ruotolo and M. H. Lim, Structure-mechanism-based engineering of chemical regulators targeting distinct pathological factors in Alzheimer's disease, *Nat. Commun.*, 2016, **7**, 13115.
22 A. K. Sharma, S. T. Pavlova, J. Kim, D. Finkelstein, N. J. Hawco, N. P. Rath, J. Kim and L. M. Mirica, Bifunctional compounds for controlling metal-mediated aggregation of the Aβ42 peptide, *J. Am. Chem. Soc.*, 2012, **134**, 6625–6636.
23 A. K. Sharma, J. Kim, J. T. Prior, N. J. Hawco, N. P. Rath, J. Kim and L. M. Mirica, Small bifunctional chelators that do not disaggregate amyloid β fibrils exhibit reduced cellular toxicity, *Inorg. Chem.*, 2014, **53**, 11367–11376.
24 H.-J. Cho, A. K. Sharma, Y. Zhang, M. L. Gross and L. M. Mirica, A Multifunctional Chemical Agent as an Attenuator of Amyloid Burden and Neuroinflammation in Alzheimer's Disease, *ACS Chem. Neurosci.*, 2020, **11**, 1471–1481.
25 A. K. Sharma, J. W. Schultz, J. T. Prior, N. P. Rath and L. M. Mirica, Coordination chemistry of bifunctional chemical agents designed for applications in ^{64}Cu PET imaging for Alzheimer's disease, *Inorg. Chem.*, 2017, **56**, 13801–13814.
26 M. E. Alberto, T. Marino, N. Russo, M. Toscano and E. Sicilia, The performance of density functional based methods in the description of selected biological systems and processes, *Phys. Chem. Chem. Phys.*, 2012, **14**, 14943–14953.
27 M. J. Frisch, G. W. Trucks, H. B. Schlegel, G. E. Scuseria, M. A. Robb, J. R. Cheeseman, G. Scalmani, V. Barone and G. A. Petersson, *et al.*, *Gaussian 09, revision D.01*, 2014.
28 Y. Zhao, N. E. Schultz and D. G. Truhlar, Design of Density Functionals by Combining the Method of Constraint Satisfaction with Parametrization for Thermochemistry, Thermochemical Kinetics, and Noncovalent Interactions, *J. Chem. Theory Comput.*, 2006, **2**, 364–382.
29 A. V. Marenich, C. J. Cramer and D. G. Truhlar, Universal Solvation Model Based on Solute Electron Density and on a Continuum Model of the Solvent Defined by the Bulk Dielectric Constant and Atomic Surface Tensions, *J. Phys. Chem. B*, 2009, **113**, 6378–6396.
30 A. Galano and J. R. Alvarez-Idaboy, A computational methodology for accurate predictions of rate constants in solution: application to the assessment of primary antioxidant activity, *J. Comput. Chem.*, 2013, **34**, 2430–2445.
31 A. Galano and J. R. Alvarez-Idaboy, Computational strategies for predicting free radical scavengers' protection against oxidative stress: where are we and what might follow?, *Int. J. Quantum Chem.*, 2019, **119**, 25665.
32 D. G. Truhlar, B. C. Garrett and S. J. Klippenstein, Current status of transition-state theory, *J. Phys. Chem.*, 1996, **100**, 12771–12782.
33 M. G. Evans and M. Polanyi, Some applications of the transition state method to the calculation of reaction velocities, especially in solution, *Trans. Faraday Soc.*, 1935, **31**, 875–882.
34 R. A. Marcus, Electron transfer reactions in chemistry: Theory and experiment (Nobel lecture), *Angew. Chem., Int. Ed. Engl.*, 1993, **32**, 1111–1121.
35 F. C. Collins and G. E. Kimball, Diffusion-controlled reaction rates, *J. Colloid Sci.*, 1949, **4**, 425–437.
36 A. Galano, A. Perez-Gonzalez, R. Castaneda-Arriaga, L. Munoz-Rugeles, G. Mendoza-Sarmiento, A. Romero-Silva, A. IbarraEscutia, A. M. Rebollar-Zepeda, J. R. Leon-Carmona, M. A. Hernandez-Olivares and J. R. Alvarez-Idaboy, Empirically Fitted Parameters for Calculating p*K*a Values with Small Deviations from Experiments Using a Simple Computational Strategy, *J. Chem. Inf. Model.*, 2016, **56**, 1714–1724.
37 S. Ahmadi, T. Marino, M. Prejanò, N. Russo and M. Toscano, Antioxidant Properties of the Vam3 Derivative of Resveratrol, *Molecules*, 2018, **23**, 2446.
38 A. Galano, G. Mazzone, R. Alvarez-Diduk, T. Marino, J. R. Alvarez-Idaboy and N. Russo, Food Antioxidants: Chemical Insights at the Molecular Level, *Annu. Rev. Food Sci. Technol.*, 2016, **7**, 335–352.
39 Z. Milanovic, J. Tosovic, S. Markovic and Z. Markovic, Comparison of the scavenging capacities of phloroglucinol and 2,4,6-trihydroxypyridine towards HO radical: a computational study, *RSC Adv.*, 2020, **10**, 43262–43272.
40 T. C. Ngo, T. H. Nguyen and D. Q. Dao, Radical Scavenging Activity of Natural-Based Cassaine Diterpenoid Amides and Amines, *J. Chem. Inf. Model.*, 2019, **59**, 766–776.
41 R. Luckaya, R. D. Hancock, I. Cukrowskia and J. H. Reibenspiesb, Study of protonation of 1,4,7-tris(2_hydroxyethyl)-1,4,7-triazacyclononane, and its complexes with metal ions, by crystallography, polarography, potentiometry, molecular mechanics and NMR, *Inorg. Chim. Acta*, 1996, **246**, 159–169.
42 M. Leopoldini, N. Russo and M. Toscano, The molecular basis of working mechanism of natural polyphenolic antioxidants, *Food Chem.*, 2011, **125**, 288–306.
43 A. Parise, B. C. De Simone, T. Marino, M. Toscano and N. Russo, Quantum Mechanical Predictions of the Antioxidant Capability of Moracin C Isomers, *Front. Chem.*, 2021, **9**, 666647.
44 A. Galano and A. Martínez, Capsaicin, a tasty free radical scavenger: Mechanism of action and kinetics, *J. Phys. Chem. B*, 2012, **116**, 1200–1208.
45 M. Spiegel, T. Marino, M. Prejanò and N. Russo, On the scavenging ability of scutellarein against the OOH radical in water and lipid-like environments: A theoretical study, *Antioxidants*, 2022, **11**, 224.
46 M. Spiegel, T. Andruniów and Z. Sroka, Flavones' and Flavonols' Antiradical Structure–Activity Relationship. A Quantum Chemical Study, *Antioxidants*, 2020, **9**, 461.
47 M. E. Alberto, N. Russo, A. Grand and A. Galano, A physicochemical examination of the free radical scavenging activity of Trolox: mechanism, kinetics and influence of the environment, *Phys. Chem. Chem. Phys.*, 2013, **15**, 4642–4650.
48 A. Pérez-González, M. Prejanò, N. Russo, T. Marino and A. Galano, Capsaicin, a powerful OH-inactivating ligand, *Antioxidants*, 2020, **9**, 1247.